PCCP

Accepted Manuscript

This is an *Accepted Manuscript*, which has been through the Royal Society of Chemistry peer review process and has been accepted for publication.

Accepted Manuscripts are published online shortly after acceptance, before technical editing, formatting and proof reading. Using this free service, authors can make their results available to the community, in citable form, before we publish the edited article. We will replace this *Accepted Manuscript* with the edited and formatted *Advance Article* as soon as it is available.

You can find more information about *Accepted Manuscripts* in the **Information for Authors**.

Please note that technical editing may introduce minor changes to the text and/or graphics, which may alter content. The journal's standard **Terms & Conditions** and the **Ethical guidelines** still apply. In no event shall the Royal Society of Chemistry be held responsible for any errors or omissions in this *Accepted Manuscript* or any consequences arising from the use of any information it contains.

Approaching 100% coverage $CH_3NH_3PbI_{3-x}Cl_x$ films with highly oriented crystal domains for reproducible and efficient planar heterojunction perovskite solar cells

Like Huang, Ziyang Hu*, Guoqiang Yue, Jinwang Liu, Xiaohong Cui, Jing Zhang, Yuejin Zhu*
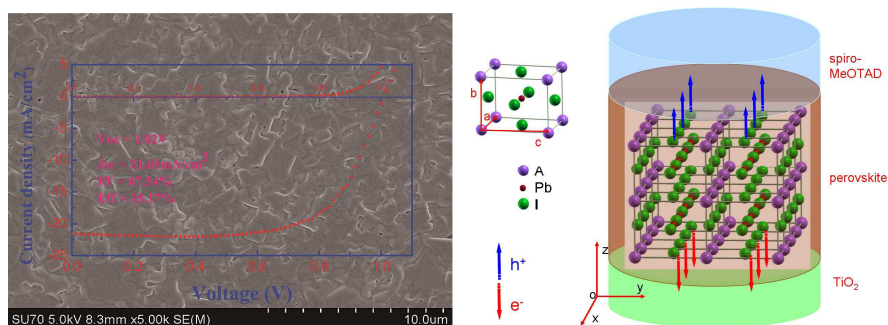
Abstract: Depositing pinhole-free perovskite films is of vital importance for achieving high performance perovskite solar cells, especially in a planar heterojunction device. Here, approaching 100% coverage perovskite films with highly oriented crystal domains were obtained by carefully controlling the annealing temperature and duration. Perovskite solar cells with an average efficiency of 12% and a maximum efficiency of 15.17% were achieved in a planar heterojunction structure. Comprehensive characterization and analysis showed that proper annealing temperature and duration allowed the perovskite crystal to grow slowly, resulting in highly oriented crystal domains without few internal voids or pinholes. Crystal perovskite possessing an anisotropic transport property ensures the efficient electrons and holes transport to their corresponding electrodes.

Introduction

Organometal trihalide perovskites ($CH_3NH_3PbX_3$, X = Cl, Br, I, and its mixed-halide perovskites $CH_3NH_3PbI_{3-x}Cl_x$) with perfect semiconducting properties[1-2] have emerged as a new generation of solution processable, low cost materials for mesoscopic or planar heterojunction (PH) solar cells and led to record breaking efficiencies.[3-7] Perovskite films can be deposited easily onto

the substrates via single or two-step reactions of precursors.[3, 5-6] Originally, metal oxides involving TiO$_2$ or Al$_2$O$_3$ were adopted as scaffold to form perovskite films in mesoporous photovoltaic devices.[3-6] Since that, PH architectures without mesoporous layers have been proposed to simplify the device architectures and processing procedures. Soon, high efficiencies have been reported, which demonstrates that a mesoporous layer is not necessary to achieve high efficient perovskite solar cells (PVK SCs).[7-8] At the same time, photo-physical studies have proven that perovskite materials exhibit several tens of nanoseconds in carrier lifetime and a few hundred nanometers in diffusion length, confirming the validity of using PH structure.[1-2] Additionally, the intrinsic bipolar transport properties of perovskite materials make them ideal for p-i-n device architectures where they serve both as the intrinsic absorption layers and carrier transport layers.[3-6] For the mixed-halide perovskites CH$_3$NH$_3$PbI$_{3-x}$Cl$_x$ system, the presence of chloride ion source in the precursor solutions results in a strong increase in the overall charge diffusion length, making it particularly suitable for PH configuration. The recent breakthrough of organometal halide perovskites based PH PVK SCs presented a power conversion efficiency (PCE) of 19.3%, which suggests an enormous potential of PH PVK SCs in terms of achieving widely commercial applications.[7]

Currently, there are two main challenges encountered in fabrication of single solution-processed perovskite films, which includes controlling the crystallization process and ensuring high quality film. Generally, the fast crystallization of perovskite materials with solvent evaporation may result in uncontrollable film morphology. The pinhole formation, poor coverage of the perovskite film may cause low-resistance shunting paths and lost light absorption thus poor performance, especially for the PH solar cells.[8] Even though the perovskite film morphology has been investigated as a function of parameters such as initial precursor concentration, the kinds of used solvents, the solvent evaporation rate, and the time and temperature of annealing, wide morphological variation has resulted in significant differences in the photovoltaic performance, regardless of differences in fabrication method and device configuration.[9-11] Actually, for the mesoporous structure where the high coverage films do not seem as a mandatory requirement for high performance.[12] However, it is proposed that high perovskite film coverage on compact TiO$_2$ is the optimum configuration for high performance in the PH architecture. H.J. Snaith *et al.* have pointed out that the dependence of perovskite coverage on a wide range of annealing temperature

from 90 ºC-170 ºC and the relationship between perovskite coverage and device performance in

PH PVK SCs.[8] However, for sufficient coverage of the surface, it is extremely sensitive to the

range of annealing temperature and duration during the well crystallization of the perovskite film.

The coverage of perovskite film and the electronic structure of perovskite crystals also have effect

on the charge transport thus the photovoltaic performance.[11-14]

Here, by deliberate controlling the annealing temperature (< 100 ºC) and duration, approaching

100% coverage $CH_3NH_3PbI_{3-x}Cl_x$ film with highly oriented crystal domains result in reproducible

and efficient PH PVK SCs. The high coverage of perovskite film ensures adequate absorption and

avoids possible short circuit. The highly oriented crystal domains are believed to promote

electrons and holes transporting efficiently to their corresponding electrodes, PH PVK SCs with

an average efficiency of 12% and a maximum efficiency of over 15 % were achieved.

Results and discussion

PH PVK SCs were fabricated with a structure of fluorine doped tin oxide (FTO)/compact

TiO_2(c-TiO_2)/$CH_3NH_3PbI_{3-x}Cl_x$ /spiro-MeOTAD/Ag. The single-step solution-processed method

was used to deposit the perovskite films. The perovskite films were treated by the

time-temperature dependent annealing (TTD) from 60 ºC to 95 ºC as shown schematically in **Fig.**

1(a). To investigate the effect of the annealing temperature and duration on perovskite films

composition and morphology, we employed X-ray diffraction (XRD), ultraviolet-visible

absorption spectroscopy (UV-vis), scanning electron microscopy (SEM) and atomic force

microscope (AFM) measurements to characterize the perovskite films formed. XRD

measurements were conducted to investigate the nature of the material formed following the

above annealing process. Normally, low annealing temperatures result in the incomplete

conversion to the perovskite. The XRD diffractograms for samples annealed at 80 ºC/35 min

exhibit typical peaks that are mainly attributed to the precursor materials. By simply drying the

films, the excess solvent is removed, while the precursor solution is insufficient to convert into the

desired perovskite film, as indicated by the presence of strong lead chloride ($PbCl_2$) XRD

diffraction peaks in **Fig.** 1(b)). Apart from the $PbCl_2$ peaks there are several peaks that remain

unidentified which may be attributed to the possible formation of byproducts such as lead (II)

oxychloride arising.[12] Increasing the annealing temperature to 85 ºC/55 min, we can see some of

the diffraction peaks disappeared, meanwhile the color of the film became similar to that of the just spin-coated film (**Fig.** S1(d)). The specific mechanism of this phenomenon related to evolution of intermediates is unclear at present. The evolved color of the perovskite films please refer to **Fig.** S1. When the temperature came to 95 ºC/65 min, a set of new peaks appeared (indicated by #), matching those reported for the $CH_3NH_3PbI_3$ crystallized in the tetragonal perovskite structure.[3,5-6] The peaks at 14.2°, 28.5°, 43.3°, and 59.0° are correspondingly assigned to the (110), (220), (330) and (440) planes, respectively. Though the diffraction peaks of lead chloride are weak, we still speculate that the conversion from precursor materials to perovskite structure is incomplete at this stage. Continue annealing at 95 ºC/75-115 min, the position of perovskite diffraction peaks remains unchanged, while the intensity of diffraction peaks change slightly. This phenomenon confirms that the crystal structure of perovskite is stably developed under this annealing condition.
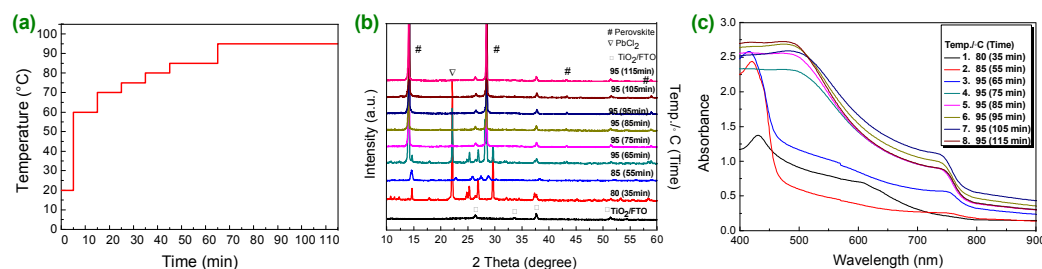

Figure 1. (a) Schematic diagram of thermal annealing method under time-temperature dependent for perovskite films, (b) X-ray diffraction patterns of compact TiO_2 films with perovskite films annealed at different stage under time-dependent temperature, (c) UV-vis absorption spectra for compact TiO_2 films with perovskite films annealed at different time.

The corresponding UV-visible absorption spectrum change of perovskite films (**Fig.** 1(c)) is consistent with that of XRD during the growth of perovskite films. At 80 ºC/35 min, no absorption peak belongs to the perovskite can be found, suggesting that precursor has not yet begun to react at this time. From 85 ºC/55 min to 95 ºC/65 min, the absorption peak 760 nm corresponding to the direct band gap transition from the first valance band to conduction band gradually emerged, implying that the perovskite growth started at this stage. At the same time, we observed that the color of film changed gradually from pale yellow to reddish brown during this period. Therefore, we suggest that the temperature ~95 ºC is critical for the perovskite growth. Continue annealing at

95 ℃, the absorption spectrum shape of the film is almost the same except for a subtle change of absorption intensity at each wavelength range, which also indicates the gradual development of perovskite crystal. By deliberate controlling the annealing temperature and duration, there is no presence of lead iodide (PbI_2) or lead chloride ($PbCl_2$) found in the final perovskite film. So we think the perovskite films were well evolved into perfect crystal. Although, we notice that the previous results have reported that the tiny remain of PbI_2 or $PbCl_2$ was existed in the perovskite film even the film is well crystallized, and the existed PbI_2 or $PbCl_2$ was beneficial for electron transportation.[15-16]
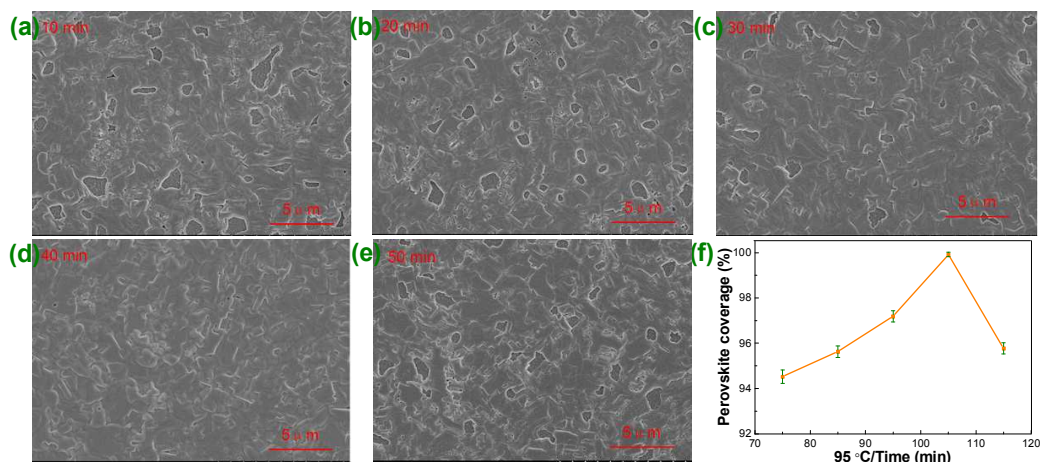

Figure 2. SEM images of compact TiO_2 films with perovskite films annealed at 95 ℃ for different time and the corresponding surface coverage as a function of annealing time.

The influence of the annealing temperature on the morphology of the perovskite films was examined by SEM. Generally, we mainly focus on the evolution of perovskite crystal structure and morphology annealed at different conditions to optimize the perovskite morphology and concerned little about the process of transition from precursor to perovskite. Since the perovskite was well crystallized at 95 ℃ as we have discussed above, here we only concentrate on examining the perovskite film annealed at this temperature for different time. **Fig.** 2 shows the SEM images of representative perovskite films annealed at 95 ℃ for different time. The calculated coverages plotted in Fig. 2 (f) were estimated from SEM images by using the threshold function in the ImageJ program, simply by setting a threshold on the image and calculating the area above and below threshold.[17] For perovskite films annealed at 95 ℃ for 10 min, many pores with rather large size can be found (**Fig.** 2 (a)). As annealing time increases, the total number of pores in the final

film decreases, meanwhile the distribution of their pore size tends to the narrow range. The film annealed at 95 ℃ for 40 min has an excellent coverage approaching 100% as few pinholes can be found (**Fig.** 2 (d)). Further increasing the anneal time (>50 min), some pinholes and small particles appeared, thus decreases the coverage (**Fig.** 2 (e)). Crystal growth is a very complex process that involves a variety of thermodynamics and energetic processes. It is proposed that non-uniform temperature leads to non-uniform grain size thus the presence of micro-holes inside the crystal, rapid heating could be one cause of non-uniform temperature. For perovskite films, slow and low heating is potentially necessary for crystal growth with few grain boundaries, microvoids, pinholes and internal stress. We got an approaching 100% coverage perovskite films with highly oriented crystal domains through appropriate control of the annealing temperature and duration. Here, combining these knowledge with our results, we propose that the anneal temperature and time of 95 ℃/40 min is ideal to obtain perovskite film with a maximum coverage.
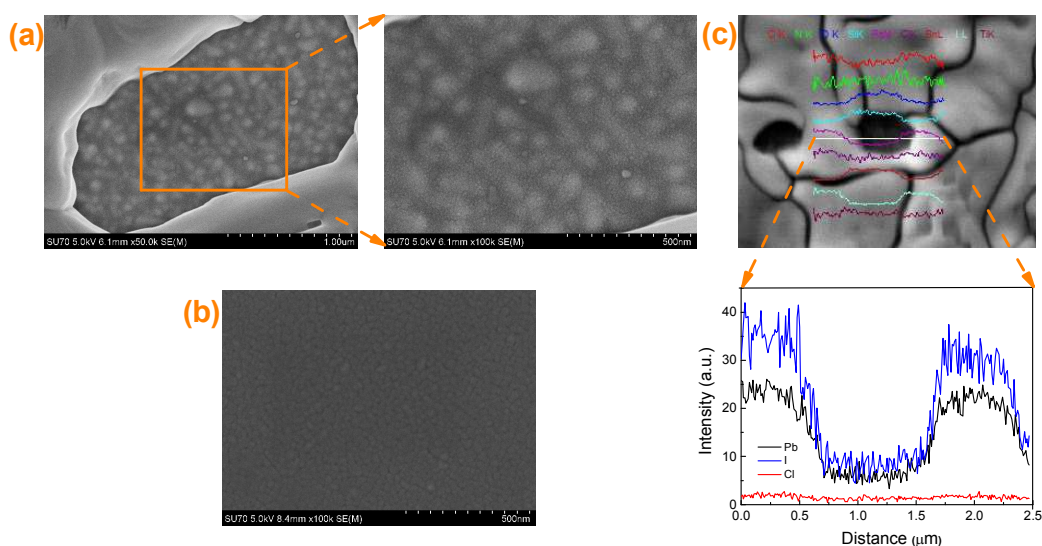

Figure 3. (a) SEM images of a pinhole of perovskite film on compact TiO_2/FTO glass substrate and (b) compact TiO_2 layer on FTO glass substrate, (c) Energy-dispersive X-ray spectroscopy of a pinhole and its adjacent areas, the scanning direction is along the white line shown from left to right.

Supposing the pinholes were uncovered by perovskite film, we calculated the surface coverage of perovskite films. It is obliged to clarify that whether those areas in pinholes are really exposed

c-TiO$_2$ or concealed c-TiO$_2$ covered by very thin perovskite film. To this end, we selected a visually better coverage perovskite sample (annealed 95 ºC for 30 min) for SEM associating with energy-dispersive X-ray spectroscopy (EDX) characterization. Compared to **Fig.** 3 (b) of only c-TiO$_2$ layer spin coated on FTO substrate, some isolated island particles with particle size ranging from 50 to 100 nm on top of the c-TiO$_2$ layer can be seen in **Fig.** 3 (a), which we believe are perovskite nanocrystalline. In order to confirm the validity of this conjecture, we examined a representative pinhole and its adjacent areas by EDX. The scanning direction is along the white line from left to right as shown in **Fig.** 3 (c). As elements with relatively small atomic weight such as hydrogen, carbon, nitrogen are not easy to be detected, only heavy elements such as lead, iodine, chlorine content are obviously detected in the test results. EDX spectra showed that lead, iodine, chlorine content are decreased significantly in the "pinhole" area, but not zero. Also, we noticed a slight reduction of carbon content as one of the constituent elements of perovskite (indicated by the red curve) in the pinhole as shown in **Fig.** 3 (c), and careful examination shows that the carbon content in the pinhole is not zero. Therefore, we believe that the island-shaped particles in the "pinhole" area should be perovskite instead of PbCl$_2$ or PbI$_2$.

On the other hand, AFM characterization shows that the average depth of the pinholes is about 300 nm (**Fig.** S2), considered together with the 350-400 nm thickness of the perovskite film extracted from the cross-sectional SEM image (**Fig.** S3) of the device, we can determine that the thickness of the discontinuous perovskite film in the pinhole is in the range of 50-100 nm, which is consistent with the above-described particle size observed by SEM. Therefore, we believe that the island-like particle in the "pinhole" area is thin film of perovskite nanocrystalline (50~100 nm). As for the specific formation mechanisms of these pinholes, more studies to further optimize the growth of perovskite film is urgently needed. With the combination of encouraging characteristics including nearly full surface coverage, large grain size, and a high degree of crystallization, we can expect promising photovoltaic performance by annealing at proper temperature. The photovoltaic performance of PH SCs was examined and the current-voltage (*J-V*) characteristics were measured under standard AM 1.5G illumination. All the performance parameters are summarized in Table 1. We can find that the device with the ideal perovskite film annealed gives the highest PCE of 15.17%, as a result of the highest open-circuit voltage (V_{OC}), fill factor (FF) and short current density (J_{SC}), 1.02 V, 21.65 mA/cm^2 and 67.54%, respectively. The

corresponding *J-V* characteristics and incident photo-current conversion efficiency (IPCE) spectra are shown in **Fig.** 4 (b, c), respectively. The calculated integrated J_{SC} value (20.92 mA/cm^2) based on the IPCE curve is very consistent with the J_{SC} value (21.65 mA/cm^2) obtained from the *J-V* curve recorded under a 100 mW/cm^2 solar simulator, as shown in Figure 4 (c). It should be noted that the observed and calculated J_{SC} values show negligible mismatch. It is reasonable that the device with perovskite film has a coverage of nearly 100% thus shows the best performance. Histograms of device efficiency (**Fig.** 4 (d)) measured for 40 separate PVK SCs show that the annealing treatment scheme mentioned above can enable achieving reproducible efficient PH PVK SCs without any further, more complex modification.

Table 1. Photovoltaic performance parameters extracted from *J-V* measurements under standard AM 1.5 G illumination of devices with perovskite films annealed at 95 ºC for different time.

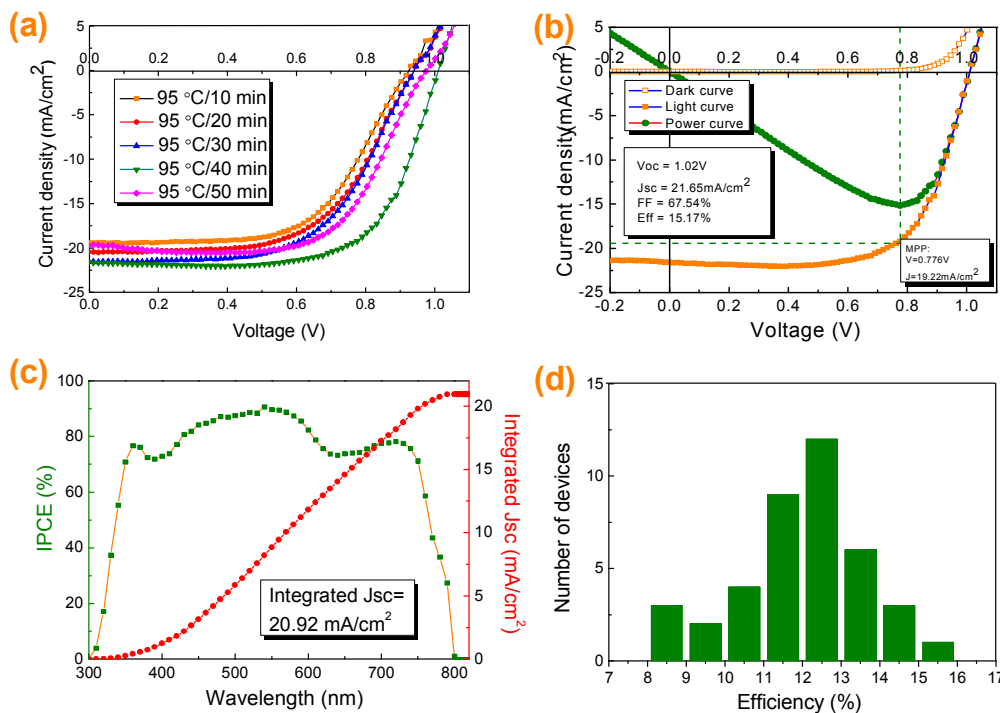| Annealing time	V_{OC} (V)	J_{SC} (mA/cm^2)	FF (%)	PCE (%)	Coverage (%)
10 min	0.917	19.35	60.34	10.89	**94.53 ± 0.30**
20 min	0.932	20.47	59.14	11.48	**95.63 ± 0.25**
30 min	0.931	21.55	59.19	12.08	**97.19 ± 0.25**
40 min	1.02	21.65	67.54	15.17	**99.85 ± 0.10**
50 min	0.974	19.71	65.41	12.77	**95.78 ± 0.25**

Figure 4. (a) Current-voltage characteristics of the corresponding devices with the perovskite films annealed at 95 ℃ for different time, (b) current-voltage curves of the best solar cell, (c) the corresponding incident photo-current conversion efficiency spectra, (d) histograms of device efficiency measured for 40 separate perovskite solar cells.

The relationship between device performance parameters and coverage of the perovskite films was then discussed. As shown in Table 1, J_{SC} shows a clear trend with coverage. At coverage of 94.53%, J_{SC} is ~19.4 mA/cm^2. As the coverage increases up to 97.19%, J_{SC} increases linearly, up to ~21.6 mA/cm^2. After that, J_{SC} increases very slowly with coverage, up to 21.65 mA/cm^2. The device V_{OC} and FF also improve with the increasing coverage, the device with the highest coverage present the best V_{OC} and FF. For efficient PH PVK SCs, a highly uniform, pinhole-free and high surface coverage perovskite film is extremely significant, as also required in other thin film solar cells.[10, 14] While the films produced by conventional spin-coating and annealing method contains larger and rod-like grains with an incomplete coverage on the substrate, which was reported in previous observations.[6] A poor coverage not only allows the light pass straightly through without absorption but also results in a high frequency of "shunt paths" that leads to direct contact between spiro-OMeTAD and the c-TiO$_2$ layer. Our study here still draw the conclusion

9

that high coverage is the necessary prerequisite for high device performance.

Besides high coverage is necessary, we believe that there are other factors contributing to the high efficiency as described below. SEM image (**Fig.** 5 (a)) shows that the perovskite film grown at 95 ºC for 40 min contains columnar crystals, whose top and bottom surfaces parallel to the electrode plane. Furthermore, XRD measurement (**Fig.** 5 (b)) shows that the resulting perovskite films onto the substrate have highly oriented crystal domains with the long c-axis preferentially oriented parallel to the substrate as the (110), (220), (330), (440) reflections are indicated.[3,4,18] Here, anisotropic electron transport properties of the perovskite crystals may contribute to the large J_{SC}.[18] As shown in **Fig.** 5(c), the XOY represents the plane of the substrate which is parallel to the TiO$_2$ electron transport layer and spiro-MeOTAD hole transport layer. The vertical axis, OZ, represents the direction perpendicular to substrate. It is well known that in the perovskite crystal, the layered organic cation and inorganic lead halide ions are alternately stacked thus constructing three-dimensional structure. The simple organic layers consisting of short-chain of organic cation help to define the degree of interaction and the properties arising in the inorganic layers. A long-chain, ordered PbI$_6$ octahedra system is actually very beneficial to the electron transport, endowing perovskite material excellent electron transport properties.[19,20] In our case, the perovskite films have highly oriented crystal domains with the long c-axis preferentially oriented parallel to the substrate. This kind of crystal domain orientation ensures that there exist countless planes of PbI$_6$ octahedra that perpendicular to the electrodes. Due to the excellent electron transport properties of the PbI$_6$ octahedra plane, electrons and holes can efficiently transport in the vertical direction across the device, and finally collected by the cathode and anode, repectively. The anisotropic charge transport properties of the perovskite crystals contribute to the increased J_{SC}, improved FF thus the PCE. For the totally low FF of the devices (< 70%), we attributed it to the mismatch of the poor conductivity of undopped c-TiO$_2$ electron transport layer and the high conductivity of spiro-MeOTAD hole transport layer with high concentration doping.[21] To further increase the overall performance of the device, using doped c-TiO$_2$ as the electron transport layer may be available.[22]
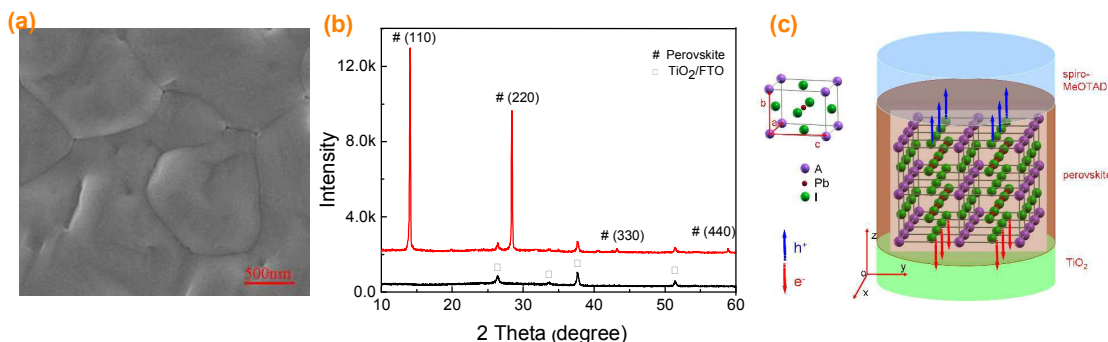
Figure 5. (a) Top view SEM image of perovskite film annealed at 95°C for 40 min, (b) XRD measurement of perovskite film annealed at 95°C for 40 min, (c) the schematic diagram of the anisotropic electron transport property of perovskite crystal, A is methylammoniu.

The perovskite films have highly oriented crystal domains with the long c-axis preferentially oriented parallel to the substrate, which is benefit to anisotropic charge carrier transport. To confirm the validity of the above hypothesis of anisotropic electron transport model, we further compared the XRD patterns of perovskite films and the performance of corresponding devices that were prepared with conventional annealing method and our optimized annealing method (TTD annealing). Fig. 6 (a, b) gives the XRD patterns of perovskite films that were treated by two different annealing methods and the *J-V* curves of corresponding devices. Fig. 6 (a) reveals that the intensity of the diffraction peak at around 14.2°, 28.5°, 43.3°, and 59.0°, which are assigned to the (110), (220), (330), and (440) lattice planes of the tetragonal perovskite structured $CH_3NH_3PbI_3$ crystals, of the perovskite film treated by the conventional annealing method is weaker than that of the perovskite film treated by the TTD annealing method. Besides that, as regard to the perovskite film that were treated by the conventional annealing method some new peaks at around 20.0°, 24.0°, 24.5°, which should be assigned to the other lattice planes of the tetragonal perovskite structured $CH_3NH_3PbI_3$ crystals, were observed. All these observed facts reveal that the optimization perovskite thin film prepared by TTD annealing method has better crystal orientation with the long c-axis preferentially oriented parallel to the substrate. Fig. 6 (b) gives the *J-V* curves of the corresponding devices revealing that the device with TTD annealing method treated perovskite films surpass that of conventional annealing method treated perovskite films in term of photovoltaic performance. This result suggests that anisotropic electronic properties of the perovskite crystals may have a great influence on the performance of the device.
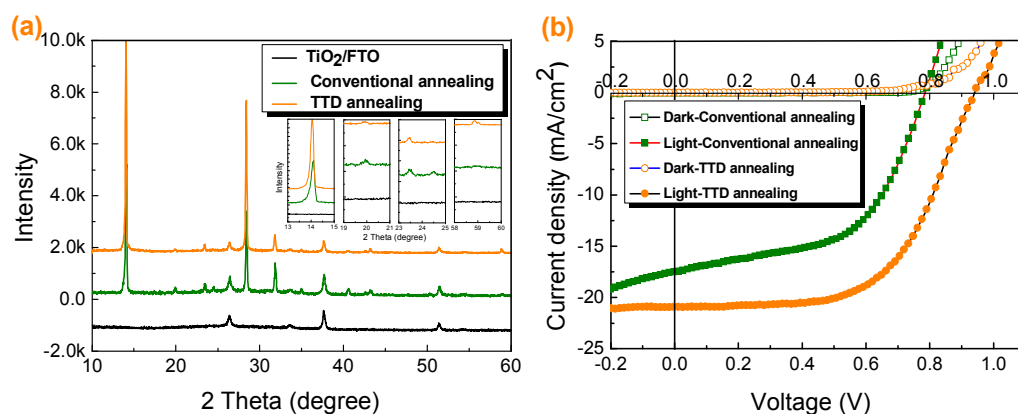
11

Figure 6. (a) XRD patterns for perovskite films annealed with different methods and the *J-V* curves of their corresponding devices.

Fig. 7 presents the plan view SEM images (a, b) of the perovskite films annealed with different methods and cross-sectional SEM images (c, d) of their corresponding devices. The perovskite film treated by conventional annealing method shows large pinholes and surface defects judging from the crystal particle sizes and film morphology (Fig. 7 (a)), while the TTD annealing method treated perovskite film was more compact and uniform (Fig. 7 (b)). This is also consistent with the XRD patterns with different diffraction intensity. The cross-sectional SEM images of the conventional annealing method treated device (Fig. 7 (c)) shows that the porous perovskite film contains irregular perovskite crystals with small sizes (~100 to 200 nm) and inevitable pores. Obviously, these pores are unfavorable for light absorption and charge transport along the film thickness direction. Specifically, such a perovskite film is actually made up of several layers of stacked grains, and this can result in many grain boundaries paralleling to the substrate which can be charge recombination centers on the path of charge transport (Fig. 7 (e)). For the TTD annealing method treated perovskite film (Fig. 7 (d)) , it was composed of densely packed perovskite grains whose grain sizes are comparable to the thickness of the film and no grain boundaries were found to be parallel to the substrate. So the perovskite film is in fact consisted of a monolayer of single crystalline grains. Thus the photogenerated charges at any spatial point of the perovskite film can transport within the densely packed columnar crystals and will not encounter grain boundaries that can easily induce charge recombination before transporting to the

corresponding electrodes (Fig. 7 (f)). Therefore, efficient electron and hole transport and collection with reduced energy loss resulted in high performance. Here, it should be emphasized that the anisotropic electron transport originals from highly oriented crystal domains and the densely packed columnar crystals are simultaneously needed for efficient charge transport and high device performance
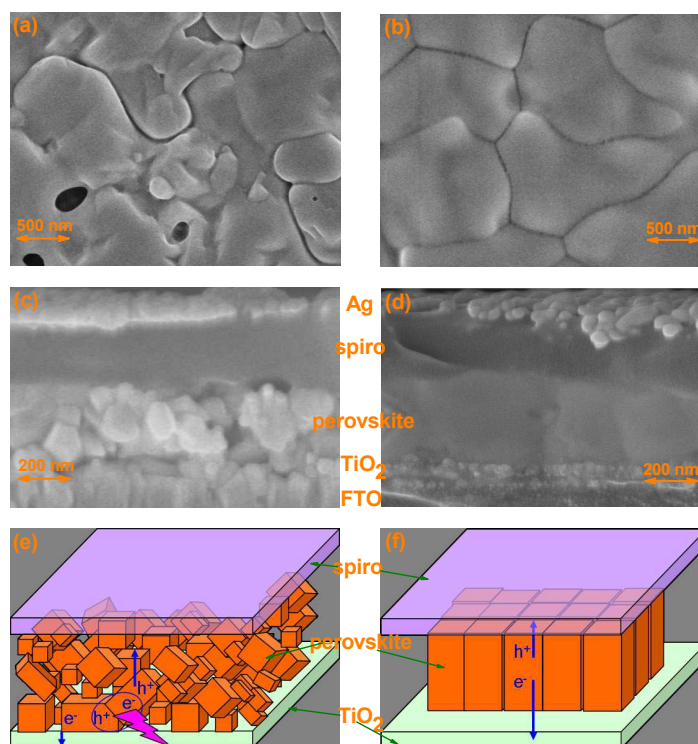

Figure 7. (a, b) Plan view SEM images of the perovskite films annealed with different methods and (c, d) cross-sectional SEM images of their corresponding devices. (e, f) charge transport model of the corresponding devices. (a, c, e) corresponds to the conventional annealing method and (b, d, f) corresponds to the TTD annealing method.

Finally, we discussed the hysteresis effect in the *J-V* measurement of the device and the device stability, the results are shown in Fig. S4. For the *J-V* measurement a canning speed of 0.03 V/s is adopted both for forward and reverse scan. As shown in Fig. S4 (a), the red and green lines represent data measured with reverse scan and forward scan, respectively, where reverse scan defines a measure from open-circuit to short-circuit and forward scan is vice versa. The device showed obvious hysteresis effect which needs further interface modification. We attribute the

anomalous hysteresis to the existed poor electronic contact between the perovskite and the charge

collection layer.[23] For stability investigation, the tested device without encapsulation was stored at

a glove box full with dry nitrogen and tested outside every 1 day for 7 days. As shown in Fig. S4

(b) the device retains 60-65% of the initial performance after 3 days, and 40-45% after 7 days,

respectively. In order to further promote the practical application of perovskite solar cells,

appropriate encapsulation is urgently needed.

Conclusions

In summary, we have demonstrated an effective growth method to fabricate perovskite films

with coverage approaching 100% by careful controlling the annealing temperature and duration. A

combination of SEM, XRD, and AFM indicated that the as-prepared perovskite film exhibits

highly uniform and oriented crystal domains. Highly reproducible PCEs of PVK SCs with an

average value of 12% and a maximum value of 15.17% were achieved in PH structure.

Anisotropic electron transport properties of the perovskite crystals have been proposed to explain

the observed photovoltaic performance. The monolayer perovskite film of columnar crystals with

highly oriented crystal domains is demonstrated to be an ideal structure for the PH PVKSCs

device which would facilitate fast charge transport. Higher reproducible performance could be

expected for PH PVK SCs with optimization of the other functional layer based on this perovskite

film growth method.

Experimental procedures

Materials

All the chemicals were used as received, including $PbCl_2$ (99.999%, Sigma-Aldrich), CH_3NH_3I

(Materwin, Shanghai), $TiCl_4$ (Sigma-Aldrich), Titanium(IV) isopropoxide (98+%, Acros),

Diethanolamine (98%, Sigma-Aldrich), spiro-OMeTAD (Lumtec), dimethylformamide (DMF),

Li-bis (trifluoromethanesulfonyl) imide (Li-TFSI, Acros), 4-tert-Butylpyridine (Sigma-Aldrich),

acetonitrile, ethanol, chlorobenzene.

Device Fabrication

First, hydrochloric acid etched, FTO-coated glass substrates (Nippon, 14 Ω/□) were cleaned by

ultrasonication in an alkaline, aqueous washing solution, rinsed with deionized water, ethanol and acetone, and subjected to an ozone-ultraviolet treatment for 15 min. A ~40 nm thick TiO_2 compact layer was then deposited on the substrates by spin-coating using a titanium diisopropoxide bis(acetylacetonate) sol-gel solution. The sol-solution was spin-coated on the substrates at 4000 rpm for 25 s, followed by annealing at 120 °C for 15 min and then 450 °C for 1 h. After cooling to room temperature, the substrates were treated in a 0.04 M aqueous solution of $TiCl_4$ for 30 min at 70 °C, rinsed with deionized water and dried at 120 °C for 15 min.

For the perovskite layer, a 1:3 ratio of $PbCl_2/CH_3NH_3I$ was mixed in DMF. Specifically, the concentration of the $PbCl_2$ and CH_3NH_3I were 0.73 and 2.2 M. The mixture solution was stirred at 60 °C overnight, and spin-coated on the FTO/c-TiO_2 substrates at 2000 rpm for 40-50 s. The single-step solution-processed method was used to deposit the perovskite films. For the time−temperature dependent annealing treatment, it is illustrated in Fig. 1(a). Generally, a transparent yellowish film forms originally once deposition of the precursor solution on the FTO/c-TiO_2 substrate is completed. Leaving the film at room temperature for several minutes, the color of the film changes to red, then becomes deep yellow and finally deep black. The final perovskite film was formed by annealing from 60 °C to 95 °C for different time. For conventional annealing method, the FTO/c-TiO_2 substrates with as spin-coated perovskite precursor layers were annealed at 100 °C for 45 min.

After the deposition of perovskite materials, a hole transport layer (HTL) solution was spin-coated at 2800 rpm for 30 s, where 1 mL spiro-OMeTAD/chlorobenzene (72.3mg/mL) solution was employed with addition of 18 μL Li-TFSI/acetonitrile (520mg/mL), and 29 μL 4-tert-butylpyridine. Finally, a 120 nm thick silver layer was thermally evaporated on top of the device under a pressure of 5×10^{-6} Torr to form the back contact. The as-fabricated device consists of 450 nm thick FTO electrode, 40 nm of TiO_2, 400 nm of perovskite, 400 nm of spiro-MeOTAD, and 120 nm of Ag.

Characterizations

X-ray diffraction pattern (2θ scans) were obtained from samples of perovskite deposited on the FTO/c-TiO_2 substrates using an X-ray diffractometer (XRD, D8 Advance, Bruker AXS, Germany), using Cu-Kα radiation (λ =1.54050Å). The UV−visible absorption spectra of the

perovskite films were recorded with a Cary 5000 UV-Vis-NIR spectrophotometer. A scanning electron microscopy (SEM, Hitachi SU-70, Japan) was used for collecting the SEM images. Atomic force microscope (AFM) was performed using Bruker Dimension 5000 Scanning Probe Microscope (SPM) in "tapping mode".

The current density-voltage (*J-V*) curves measurements were conducted with an AM 1.5 solar simulator equipped with a 1000 W xenon light source and an AM 1.5G type filter (Newport, 81904, USA). The light intensity of the solar simulator was adjusted by using a standard Si cell. *J-V* curves were obtained by applying an external bias to the cell, and measurements were recorded with a Keithley model 2400 digital source meter. The effective area of the cell was defined to be 0.04 cm^2 using a nonreflective metal mask.

The incident photo-current conversion efficiency (IPCE) spectra were measured in air on a Newport 2936-c power meter under the irradiation of a 300 W xenon light source with an Oriel Cornerstone 260 1/4 monochromator in DC mode. A reference scan with the Si detector was taken prior to the sample measurement, to allow the background to be subtracted.

Notes and references

Department of Microelectronic Science and Engineering, Ningbo Collabrative Innovation Center of Nonlinear Harzard System of Ocean and Atmosphere, Ningbo University, Ningbo, 315211, China

* Corresponding author. Tel.: +86 574 87600770; Fax: +86 574 87600744.

E-mail addresses: huziyang@nbu.edu.cn (Z. Hu), zhuyuejin@nbu.edu.cn (Y. Zhu)

1. S. D. Stranks, G. E. Eperon, G. Grancini, C. Menelaou, M. J. P. Alcocer, T. Leijtens, L. M.

Herz, A. Petrozza and H. J. Snaith, *Science*, 2013, **342**, 341-344.

2. G. C. Xing, N. Mathews, S. Y. Sun, S. S. Lim, Y. M. Lam, M. Gratzel, S. Mhaisalkar and T. C. Sum, *Science*, 2013, **342**, 344-347.

3. A. Kojima, K. Teshima, Y. Shirai and T. Miyasaka, *J. Am. Chem. Soc.*, 2009, **131**, 6050.

4. M.M. Lee, J. Teuscher, T. Miyasaka, T.N. Murakami and H.J. Snaith, *Science*, 2012, **338**, 643.

5. M. Z. Liu, M. B. Johnston and H. J. Snaith, *Nature*, 2013, **501**, 395-398.

6. J. Burschka, N. Pellet, S. J. Moon, R. Humphry-Baker, P. Gao, M. K. Nazeeruddin and M. Gratzel, *Nature*, 2013, **499**, 316-320.

7. H. P. Zhou, Q. Chen, G. Li, S. Luo, T. B. Song, H. S. Duan, Z. R. Hong, J. B. You, Y. S. Liu and Y. Yang, *Science*, 2014, **345**, 542-546.

8. G. E. Eperon, V. M. Burlakov, P. Docampo, A. Goriely and H. J. Snaith, *Adv Funct Mater.*, 2014, **24**, 151-157.

9. Q. Chen, H. P. Zhou, Z.R. Hong, S. Luo, H. S. Duan, H. H. Wang, Y. S. Liu, Ga. Li and Y. Yang, *J. Am. Chem. Soc.*, 2013, **136**, 622-625.

10. M. Saliba, K. W. Tan, H. Sai, D. T. Moore, T. Scott, W. Zhang, L. A. Estroff, U. Wiesner, and H. J. Snaith, *J. Phys. Chem. C*, 2014, **118,** 17171-17177.

11. R. Kang, J. E. Kim, J. S. Yeo, S. Lee, Y. J. Jeon and D.Y. Kim, *J. Phys. Chem. C*, 2014, **118**, 26513-26520.

12. A. Dualeh, N. Tétreault, T. Moehl, P. Gao, M.K. Nazeeruddin and M.Grätzel, *Adv. Funct. Mater.*, 2014, **24**, 3250.

13. Y. Z. Wu, A. Islam, X. D. Yang, C. J. Qin, J. Liu, K. Zhang, W. Q. Peng and L. Y. Han, *Energ Environ Sci.*, 2014, **7**, 2934-2938.

14. M. Xiao, F. Huang, W. Huang, Y. Dkhissi, Y. Zhu, J. Etheridge, A. Gray-Weale, U. Bach, Y. B. Cheng and L. Spiccia, *Angew. Chem. Int. Ed.*, 2014, **126**, 10056.

15. D. H. Cao, C. C. Stoumpos, C. D. Malliakas, M. J. Katz, O. K. Farha, J. T. Hupp and M.G. Kanatzidis, *APL Materials*, 2014, **2**, 091101.

16. N. Li, H.P. Dong, H. Dong, J.L. Li, W.Z. Li, G.D. Niu, X.D. Guo, Z.X. Wu and L.D. Wang, *J. Mater. Chem. A*, 2014, **2**, 14973.

17. W. Rasband, ImageJ 2005, http://rsb.info.nih.gov/ij/, accessed: November 2014.

18. P. Docampo, F. C. Hanusch, N. Giesbrecht, P. Angloher, A. Ivanova and T. Bein, *APL*

Materials,2014, **2**, 081508.

19.   D. B. Mitzi, K.Chondroudis, C. R. Kagan, *IBM journal of research and development*, 2001, **45**, 29-45.

20.   T. Baikie, Y.N. Fang, J. M. Kadro, M. Schreyer, F.X. Wei, S. G. Mhaisalkar, M. Graetzel and T. J. White, *J. Mater. Chem. A*, 2013, **1**, 5628.

21.   J. H. Noh, N. J. Jeon, Y. C. Choi, M. K. Nazeeruddin, M. Gratzel and S. Seok *J. Mater. Chem. A*, 2013, **1**, 11842.

22.   K. Manseki, T. Ikeya, A. Tamura, T. Ban, T. Sugiura and T. Yoshida, *RSC Adv.*, 2014, **4**, 9652.

23.   C. Tao, S. Neutzner, L. Colella, S. Marras, A. R. Srimath Kandada, M. gandini, M. De Bastiani, G. Pace, L. Manna, M. Caironi, C. Bertarelli and A. petrozza, *Energy Environ. Sci.,* 2015, DOI: 10.1039/C5EE01720C.